EARTHQUAKE ENGINEERING AND STRUCTURAL DYNAMICS
Earthquake Engng. Struct. Dyn. **27**, 1069–1093 (1998)

SEISMIC RESPONSE ANALYSIS OF BRIDGES ISOLATED WITH FRICTION PENDULUM BEARINGS

YEN-PO WANG[1,*], LAP-LOI CHUNG[2], AND WEI-HSIN LIAO[1]

[1] *Department of Civil Engineering, National Chiao-Tung University, Hsinchu, Taiwan, R.O.C.*
[2] *National Center for Research on Earthquake Engineering, National Taiwan University, Taipei, Taiwan, R.O.C.*

SUMMARY

A systematic method is developed for the dynamic analysis of the structures with sliding isolation which is a highly non-linear dynamic problem. According to the proposed method, a unified motion equation can be adapted for both stick and slip modes of the system. Unlike the traditional methods by which the integration interval has to be chopped into infinitesimal pieces during the transition of sliding and non-sliding modes, the integration interval remains constant throughout the whole process of the dynamic analysis by the proposed method so that accuracy and efficiency in the analysis of the non-linear system can be enhanced to a large extent. Moreover, the proposed method is general enough to be adapted for the analysis of the structures with multiple sliding isolators undergoing independent motion conditions simultaneously. The superiority of the proposed method for the analysis of sliding supported structures is verified by a three-span continuous bridge subjected to harmonic motions and real earthquakes. In addition, the side effect of excessive displacement of the superstructure induced by the sliding isolation is eliminated by replacing one of the roller supports on the abutments with hinge support. Therefore, both reductions in the forces of the substructure and the displacements of the superstructure can be achieved simultaneously. © 1998 John Wiley & Sons, Ltd.

KEY WORDS: dynamic analysis; sliding isolation; bridges; seismic response; friction pendulum bearings

INTRODUCTION

Bridges are vulnerable when subjected to severe earthquakes. Although considerable progress has been made in earthquake engineering towards the end of the century, catastrophic bridge failure examples are found wherever large-scale earthquakes attack. Damage of the bridge structures occur primarily in the piers, which may in turn result in collapse of the bridge spans. Although the ductility design concept has been widely accepted for seismic design of structures in engineering practice, this may not be appropriate for bridges since they are short of structural redundancy in nature. Besides, ultimate strength design does not seem to work for bridge structures as often the piers are found to fail in shear rather than flexure. The effort on protection of bridges against earthquakes should therefore be focused on minimizing the forces to be carried by the piers, in particular the shears. Seismic isolation is conceivably one of the most promising alternatives in this regards. Isolation systems are basically typified into rubber bearings and sliding bearings. Rubber bearings with high lateral flexibility are meant to shift the vibrational periods of the structures so as to avoid resonance with the excitations; they are usually combined with high damping material to prevent the isolated structures from over-displacing. Sliding bearings are introduced to filter out the imparting earthquake forces through the frictional interfaces. This type of systems rarely possess re-centering capability, except the Friction Pendulum Bearings (FPB) which, with curved sliding surfaces, can provide the isolated structures

* Correspondence to: Yen-Po Wang, Department of Civil Engineering, National Chiao-Tung University, 1001 Ta Hsueh Road, Hsinchu, Taiwan, Republic of China

Contract/grant sponsor: National Science Council of the Republic of China; Contract/grant number: NSC 84-2221-E-009-008

CCC 0098–8847/98/101069–25$17·50

Received 3 May 1997
Revised 9 March 1998

with restoring forces by gravity. Although rubber bearings have been extensively used in base isolation systems, sliding bearings have found more and more applications in recent years for economic reasons.[1–4]

Dynamics of sliding structures is a highly non-linear problem due to friction mechanism. Analytical solutions are complicated and restricted to harmonic motions for systems with no more than two degrees of freedom, under idealized conditions.[5,6] More realistic transient responses to MDOF sliding systems can only be obtained numerically. Mostaghel *et al.*[7] propose a semi-analytical procedure by interchangingly using two sets of governing equations corresponding to sliding and non-sliding motion conditions. Yang *et al.*[8] propose a numerical solution by adding to the foundation floor a fictitious spring to represent the frictional effect of the sliding bearings. In order to retain the non-linear characteristic of the friction mechanism with appreciable accuracy, both the methods require to chop the integration interval into infinitesimal pieces during the transitions between sliding and non-sliding modes. Moreover, these methods are not sufficient in dealing with multiply-supported structures where the isolation bearings are undergoing different motion conditions simultaneously, as for generic isolated bridges.

The objective of this paper is to investigate the feasibility of using the FPB for seismic isolation of bridges. The problem of dynamic analysis for the highly non-linear system is tackled by introducing a logically simple and computationally efficient procedure. The motion equations for the stick and slip modes of the sliding isolated structure are unified into a single equation in state-space form such that the integration interval remains constant throughout the whole process of analysis. Moreover, the proposed method is so general that it can be adapted for the analysis of the structures with multiple sliding isolators undergoing independent motion conditions simultaneously. Rigorous assessment of bridges with seismic isolation is carried out by a three-span continuous bridge subjected to harmonic motions and real earthquakes.

MODELLING OF FRICTION PENDULUM BEARINGS

A seismically isolated bridge consists primarily of the superstructure, the isolators, and the substructure (or piers), three basic components. In this study, the seismic isolators considered are the Friction Pendulum Bearings (FPBs). The upper plate of the FPB is attached under the bridge superstructure, whereas its lower plate is mounted on top of the pier. The bridge superstructure isolated by FPBs may slide under earthquake excitations. Once the sliding commences, it is simultaneously raised up along the curved surface of the FPB. As shown in Figure 1(a), the relative displacement between the sliding interfaces is $(u_1 - u_2)$ and the potential energy V_g due to gravity accumulated during the lift-up is

$$V_{\mathrm{g}} = WR(1 - \cos\theta) = WR\left[1 - \sqrt{1 - \left(\frac{u_1 - u_2}{R}\right)^2}\right] \tag{1}$$

where W is the weight supported by the bearing, R is the radius of curvature of the sliding surface and θ is the sliding angle, as depicted in Figure 1(b). No strain energy is accumulated during this rigid-body sliding motion.

Since the amount of sliding displacement of the bearing is practically far less than the radius of curvature R, the potential energy can be reasonably approximated as

$$V_{\mathrm{g}} \approx \frac{WR}{2}\left(\frac{u_1 - u_2}{R}\right)^2 \tag{2}$$

The stiffness matrix K_{FPB} of the pendulum in the form of a finite element is then obtained by taking a variation of the potential energy (2) based on virtual work principles as

$$K_{\mathrm{FPB}} = \begin{bmatrix} \dfrac{W}{R} & -\dfrac{W}{R} \\ -\dfrac{W}{R} & \dfrac{W}{R} \end{bmatrix} \tag{3}$$

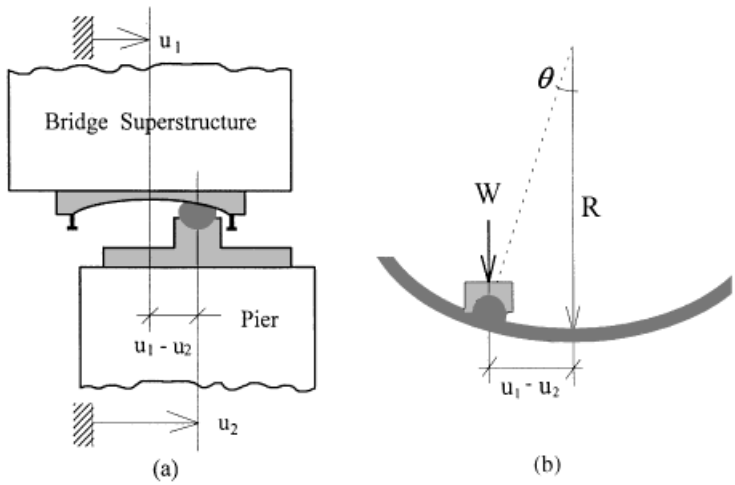

Figure 1. Illustrative diagram of friction pendulum bearing

Note from equation (3) that the larger the radius of curvature the smaller the lateral stiffness is provided by the bearing. As the radius of curvature approaches infinity, K_{FPB} becomes a null matrix indicating a complete loss of its restoring capability, as in the case of a flat-type sliding bearing.

The friction force between the sliding interfaces, on the other hand, plays the role of energy dissipating during the sliding motion. The motion of the friction bearings can be resolved into the following modes:

(a) *Stick mode*. This occurs when the ground-motion-induced shear forces between the sliding interfaces of the bearing fail to overcome the maximum friction force. In such occasions, the relative velocity between the interfaces is zero.
(b) *Slip mode*. When the ground-motion-induced shear force reaches the maximum friction force of the sliding interfaces, the bearing takes no more shear and is then forced to slide.

Under the assumption of small sliding displacement ($\theta \ll 1$), the friction force acting along the sliding surfaces is governed by

$$|f| \leqslant \mu W \tag{4}$$

where μ is the coefficient of friction. This coefficient can be either a constant as considered in Coulomb's model, or dependent on the sliding velocity and the bearing pressure as proposed by Mokha and Constantinou[9,10] for Teflon-steel interfaces as

$$\mu = \mu_{max} - (\mu_{max} - \mu_{min}) \exp(-a|\dot{u}_1 - \dot{u}_2|) \tag{5}$$

where μ_{max} and μ_{min} are, respectively, the maximum and the minimum values of the coefficient of friction, and the coefficient a is to be determined from the bearing pressure. The non-sliding conditions for the bearing are

$$|f| < \mu W \quad \text{and} \quad \dot{u}_1 - \dot{u}_2 = 0 \tag{6}$$

and sliding occurs only if

$$f = \mu W \operatorname{sgn}(\dot{u}_1 - \dot{u}_2) \tag{7}$$

where *sgn* denotes the signum function.

SOLUTION ALGORITHM FOR NONLINEAR DYNAMIC ANALYSIS

The equation of motion of a seismic-isolated bridge structure under earthquake loads $\mathbf{w}(t)$ can be represented as

$$\mathbf{M}\ddot{\mathbf{u}}(t) + \mathbf{C}\dot{\mathbf{u}}(t) + \mathbf{K}\mathbf{u}(t) = \mathbf{B}\mathbf{F}(t) + \mathbf{E}\mathbf{w}(t) \tag{8}$$

where $\mathbf{u}(t)$ is the $n \times 1$ displacement vector, $\mathbf{M}$, $\mathbf{C}$, $\mathbf{K}$ are, respectively, the $n \times n$ mass, damping and stiffness matrices, $\mathbf{E}$ is the $n \times 1$ location matrix of the excitation loads, $\mathbf{B}$ is the $n \times q$ location matrix of the friction forces and $\mathbf{F}(t)$ is the $q \times 1$ friction vector with its entries satisfying the conditions described in equations (6) or (7).

State-space procedure

Equation (8) can be represented in a state-space form, leading to a first-order differential equation as

$$\dot{\mathbf{z}}(t) = \mathbf{A}^*\mathbf{z}(t) + \mathbf{B}^*\mathbf{F}(t) + \mathbf{E}^*\mathbf{w}(t) \tag{9}$$

where

$\mathbf{z}(t) = \begin{bmatrix} \mathbf{u}(t) \\ \dot{\mathbf{u}}(t) \end{bmatrix}$ is the $n \times 1$ state vector,

$\mathbf{A}^* = \begin{bmatrix} \mathbf{0} & \mathbf{I} \\ -\mathbf{M}^{-1}\mathbf{K} & -\mathbf{M}^{-1}\mathbf{C} \end{bmatrix}$ is the $2n \times 2n$ system matrix,

$\mathbf{B}^* = \begin{bmatrix} \mathbf{0} \\ \mathbf{M}^{-1}\mathbf{B} \end{bmatrix}$ is the $2n \times q$ friction load matrix, and

$\mathbf{E}^* = \begin{bmatrix} \mathbf{0} \\ \mathbf{M}^{-1}\mathbf{E} \end{bmatrix}$ is the $2n \times 1$ earthquake load matrix.

Taking a Laplace transformation of equation (9), it gives

$$\mathbf{z}(s) = \mathbf{H}(s)\mathbf{z}(t_0) + \mathbf{H}(s)\mathbf{G}(s) \tag{10}$$

where $\mathbf{z}(t_0)$ denotes the initial conditions of the state at $t = t_0$, and

$$\mathbf{H}(s) = (s\mathbf{I} - \mathbf{A}^*)^{-1} \tag{11}$$

$$\mathbf{G}(s) = \mathbf{B}^*\mathbf{F}(s) + \mathbf{E}^*\mathbf{w}(s) \tag{12}$$

The solution of the time-invariant dynamic system is then obtained by transforming equation (10) back to the time domain, giving

$$\mathbf{z}(t) = \mathrm{e}^{\mathbf{A}^*(t-t_0)}\mathbf{z}(t_0) + \int_0^t \mathrm{e}^{\mathbf{A}^*(t-\tau)}\left[\mathbf{B}^*\mathbf{F}(\tau) + \mathbf{E}^*\mathbf{w}(\tau)\right]\mathrm{d}\tau \tag{13}$$

In order to carry out the integration involved in equation (13), the continuous-time evolutions of $\mathbf{w}(\tau)$ and $\mathbf{F}(\tau)$ between the sampling interval are required. Since the recorded earthquake load functions are commonly discrete and the friction forces are piecewise linear in nature, it is reasonable to assume linear variations of these loading functions between two consecutive sampling instants. That is

$$\mathbf{F}(\tau) = \frac{k\Delta t - \tau}{\Delta t}\mathbf{F}[(k-1)\,\Delta t] + \frac{\tau - (k-1)\,\Delta t}{\Delta t}\mathbf{F}[k\,\Delta t], \quad (k-1)\,\Delta t \leqslant \tau \leqslant k\,\Delta t \tag{14a}$$

$$\mathbf{w}(\tau) = \frac{k\Delta t - \tau}{\Delta t}\mathbf{w}[(k-1)\,\Delta t] + \frac{\tau - (k-1)\,\Delta t}{\Delta t}\mathbf{w}[k\,\Delta t], \quad (k-1)\,\Delta t \leqslant \tau \leqslant k\,\Delta t \tag{14b}$$

When $t_0 = (k-1)\,\Delta t$, $t = k\,\Delta t$, and $\mathbf{z}[k] = \mathbf{z}(k\,\Delta t)$, $\mathbf{F}[k] = \mathbf{F}(k\,\Delta t)$, … , etc. are assigned, from equation (13), the analytical solution to the state equation (9) is a difference equation as

$$\mathbf{z}[k] = \mathbf{A}\mathbf{z}[k-1] + \mathbf{B}_0\mathbf{F}[k-1] + \mathbf{B}_1\mathbf{F}[k] + \mathbf{E}_0\mathbf{w}[k-1] + \mathbf{E}_1\mathbf{w}[k] \tag{15}$$

where

$\mathbf{A} = e^{\mathbf{A}^*\Delta t}$ is the $2n \times 2n$ discrete-time system matrix,

$\mathbf{B}_0 = [(\mathbf{A}^*)^{-1}\mathbf{A} + \dfrac{1}{\Delta t}(\mathbf{A}^*)^{-2}(\mathbf{I} - \mathbf{A})]\mathbf{B}^*$ is the $2n \times q$ discrete-time friction loading matrix of the previous time step,

$\mathbf{B}_1 = [-(\mathbf{A}^*)^{-1} + \dfrac{1}{\Delta t}(\mathbf{A}^*)^{-2}(\mathbf{A} - \mathbf{I})]\mathbf{B}^*$ is the $2n \times q$ discrete-time friction loading matrix of the current time step,

$\mathbf{E}_0 = [(\mathbf{A}^*)^{-1}\mathbf{A} + \dfrac{1}{\Delta t}(\mathbf{A}^*)^{-2}(\mathbf{I} - \mathbf{A})]\mathbf{E}^*$ is the $2n \times 1$ discrete-time earthquake loading matrix of the previous time step, and

$\mathbf{E}_1 = [-(\mathbf{A}^*)^{-1} + \dfrac{1}{\Delta t}(\mathbf{A}^*)^{-2}(\mathbf{A} - \mathbf{I})]\mathbf{E}^*$ is the $2n \times 1$ discrete-time earthquake loading matrix of the current time step.

Shear balance method

Note that in equation (15) the friction vector $\mathbf{F}[k]$ is dependent on the motion conditions which, however, is not known as *a priori*. Therefore, the solution cannot be obtained directly through simple recursive calculations. Instead, an iterative procedure based on the concept of corrective pseudo-force is required.

The friction mechanism stated earlier reveals that the shear force and the relative velocity between the bearing's sliding interfaces are indicators of the motion conditions. For bearings that are in the sliding phase, their friction forces are defined as in equation (7) by

$$F_i = \mu_i W_i \operatorname{sgn}(\dot{u}_r^i) \tag{16}$$

where μ_i is the friction coefficient of the ith bearing, W_i is the weight supported by the ith bearing, and u_r^i is the relative velocity of the ith bearing. Yet for those in the stick phase, the shear forces are less than the corresponding maximum friction forces of the bearings. It is seen from equation (15) that for a given friction vector $\mathbf{F}[k]$ we obtain a state vector $\mathbf{z}[k]$, from which the relative velocities between the bearing are calculated. Therefore these velocity quantities may be viewed as functions of the shear forces, that is

$$\dot{u}_r^i = G_i(\mathbf{F}), \quad i = 1, \ldots, q \tag{17}$$

The key step of the proposed numerical scheme is that, at every time-step, the iterative procedure always starts by assuming all the bearings are in stick mode. This implies the conditions

$$G_i(\mathbf{F}) = 0, \quad i = 1, \ldots, q \tag{18}$$

should be satisfied. In other words, the task is first to find a set of shear forces $\mathbf{F}(k)$ that would block all the bearings from sliding. If conditions (18) are not met for any $i \in (1, \ldots, q)$, then the anticipated non-sliding conditions have not achieved for all bearings. Then the components F_i's of $\mathbf{F}[k]$ are revised according to

$$F_i^{n+1} = F_i^n - \frac{F_i^n - F_i^{n-1}}{G_i(\mathbf{F}^n) - G_i(\mathbf{F}^{n-1})} G_i(\mathbf{F}^n), \quad i = 1, \ldots, q; \quad n = 1, 2, 3, \ldots \tag{19}$$

substituted for response calculation iteratively until all $G_i(\mathbf{F})$'s converge. The resulted shear forces in the stick phases, according to the friction law however, are below the corresponding maximum friction forces $f^i_{\max}$ defined for each bearing by

$$f^i_{\max} = \mu_i W_i, \quad i = 1, \ldots, q \tag{20}$$

If this is the case, that is

$$|F_i| < \mu_i W_i, \quad \text{for all } i \tag{21}$$

then all the bearings are in stick mode as expected. However, if any of the F_i's are exceeding their corresponding maximum friction forces, these over-sheared bearings are actually in sliding phase with their shears defined by equation (16) to comply with the friction law. Then, the next step is to reset the shears for those bearings in sliding accordingly, and modify the shears by equation (19) for the rest bearings in stick mode, if any. This iterative solution algorithm is summarized below:

Step 1: Initialize $\mathbf{F}[k]$.
Step 2: Substitute $\mathbf{F}[k]$ into equation (15), get the state vector $\mathbf{z}[k]$.
Step 3: Calculate $\dot{u}^i_r$, $i = 1, \ldots, q$ from $\mathbf{z}[k]$.
Step 4: If $|\dot{u}^i_r| < \varepsilon$ (tolerance of error) for all i, go to step 6;
otherwise, modify F_i's by equation (19).
Step 5: Repeat Steps 2–4.
Step 6: If $|F_i| > \mu_i W_i$ for any $i \in (1, \ldots, q)$, replace these shear forces by $F_i = \mu_i W_i \operatorname{sgn}(\dot{u}^i_r)$ into equation (15) and modify F_j for $J \in (1, \ldots, q)$, $j \neq i$ by equation (19) iteratively until all $\dot{u}^j_r$'s converge to 0.
otherwise, terminate the iteration.
Step 7: Proceed to Step 1 for next time step.

The advantages of this proposed algorithm over the existing methods[7,8] are:

(a) It allows for a more systematic analysis and less computational efforts with a unified governing equation considered for both stick and slip modes as well as a constant integration interval.
(b) It is adaptive in dealing with systems with multiple bearings undergoing independent motion conditions simultaneously.

NUMERICAL VERIFICATIONS

Response to harmonic excitation

As an effort to verify the adequacy of the proposed numerical procedure, the harmonic response of a three-span continuous bridge [Figure 2(a)] is first investigated. Member properties of the model bridge are summarized in Table I. The harmonic excitation is expressed as $P(t) = U \sin \Omega t$ with U being the amplitude of ground acceleration and Ω the excitation frequency. Having been isolated with FPB, the whole bridge span is completely separated from the sub-structures as shown in Figure 2(b).

Assuming the friction mechanism is of Coulomb's type with friction coefficient $\mu = 10$ per cent, the sliding displacement (u) of the friction bearing normalized with respective to the peak ground displacement ($\Omega^2 U$) under non-resonant condition ($\Omega/\omega_1 = 0{\cdot}6$) is presented in Figure 3(a) and the corresponding friction hysteresis is shown in Figure 3(b). The friction hysteresis exhibits the exact non-linear pattern as assumed by Coulomb,[11] with a constant time mesh of $\Delta t = 0{\cdot}01$ sec used throughout the analysis. When the friction mechanism is assumed to be of Mokha's type with $\mu_{\max} = 10$ per cent and $\mu_{\min} = 7{\cdot}2$ per cent, the normalized bearing displacement and the corresponding friction hysteresis are presented in Figure 4(a) and 4(b), respectively. Although the bearing displacement does not show remarkable difference from the previous case, the friction hysteresis again exhibits the desired non-linear pattern as described by Mokha.[9,10]

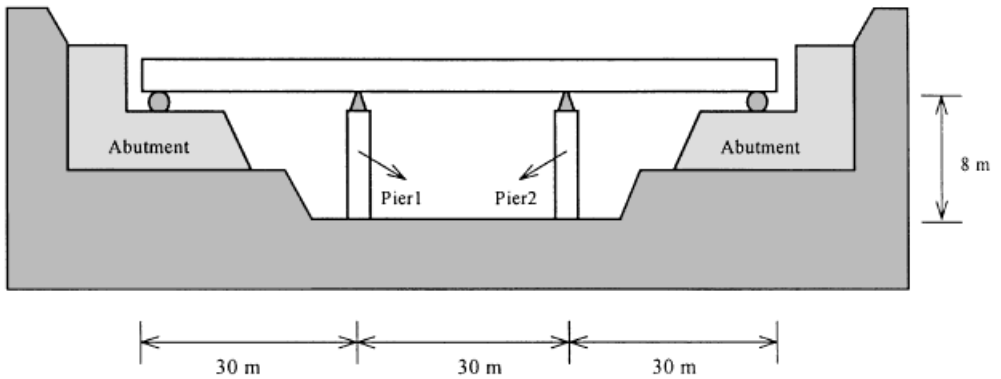

(a) Conventional

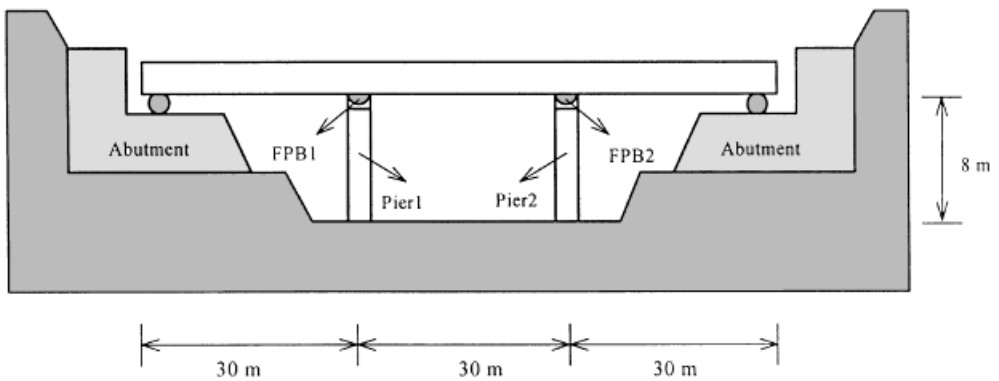

(b) Isolated (Without constraint)

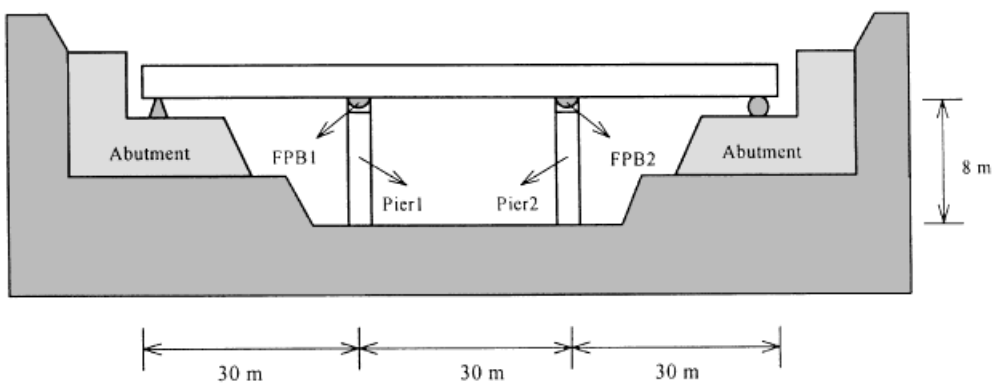

(c) Isolated (With constraint)

Figure 2. Analytical model for a three-span continuous bridge

Table I. Bridge member properties

	Superstructure	Piers
Area (m^2)	3·57	4·09
Moment of Inertia (m^4)	2·08	0·64
Young's modulus (N/m^2)	20·67E9	20·67E9
Density (T/m^3)	2·4	2·4

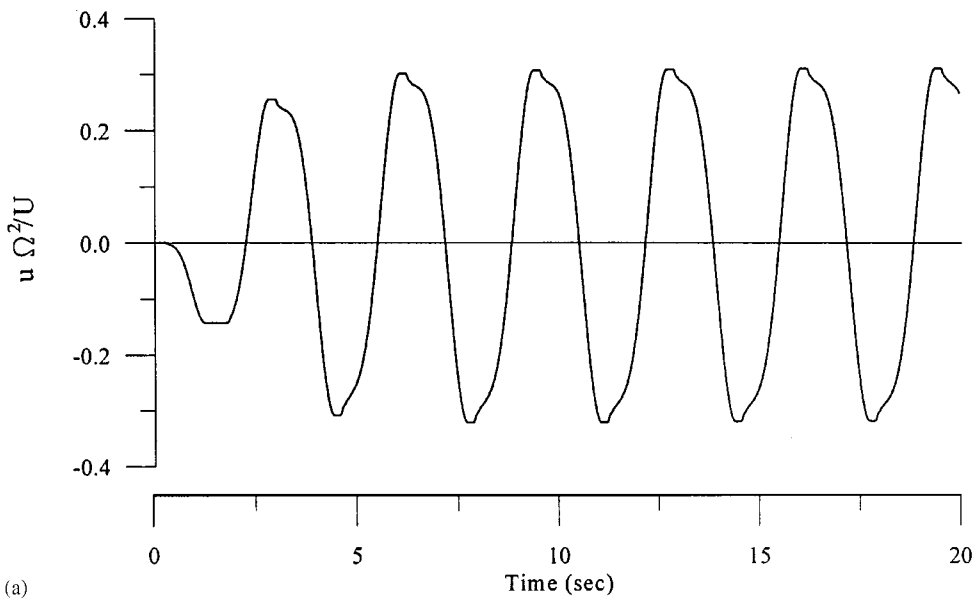

(a)

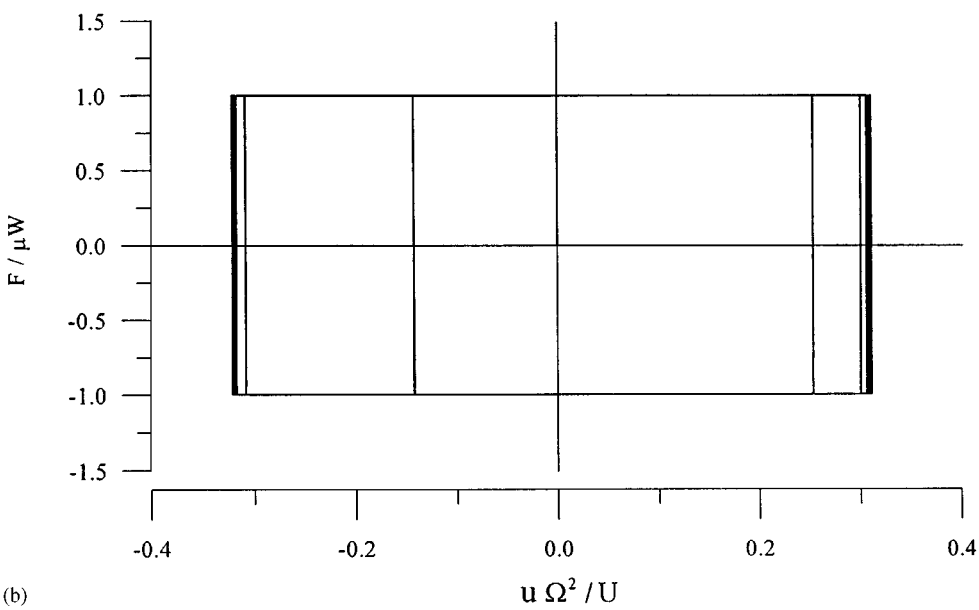

(b)

Figure 3. (a) Bearing displacement ($\Omega/\omega_1 = 0{\cdot}6$; $U/\mu g = 1$; Coulomb's model); (b) Hysteresis of friction ($\Omega/\omega_1 = 0{\cdot}6$; $U/\mu g = 1$; Coulomb's model)

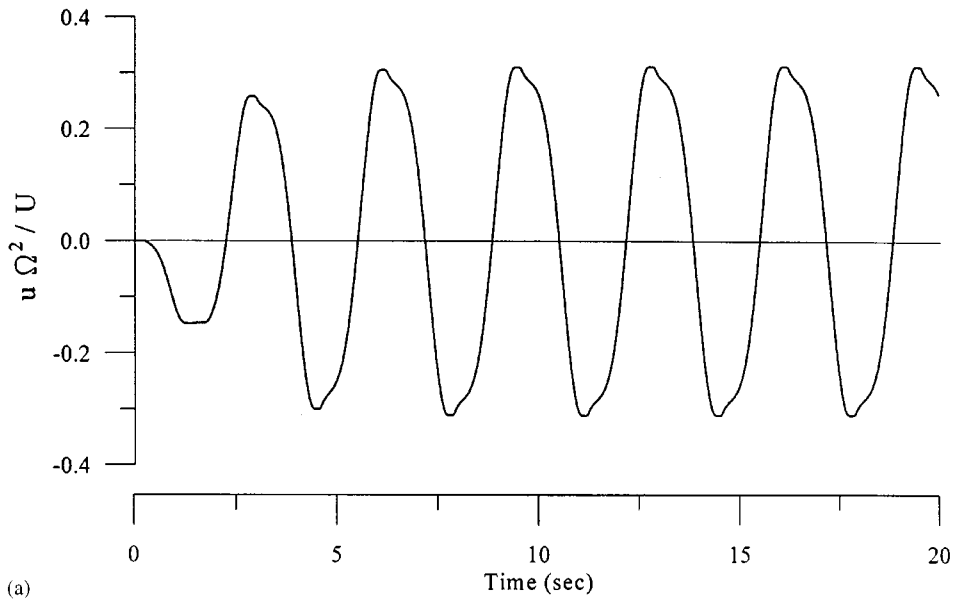

(a)

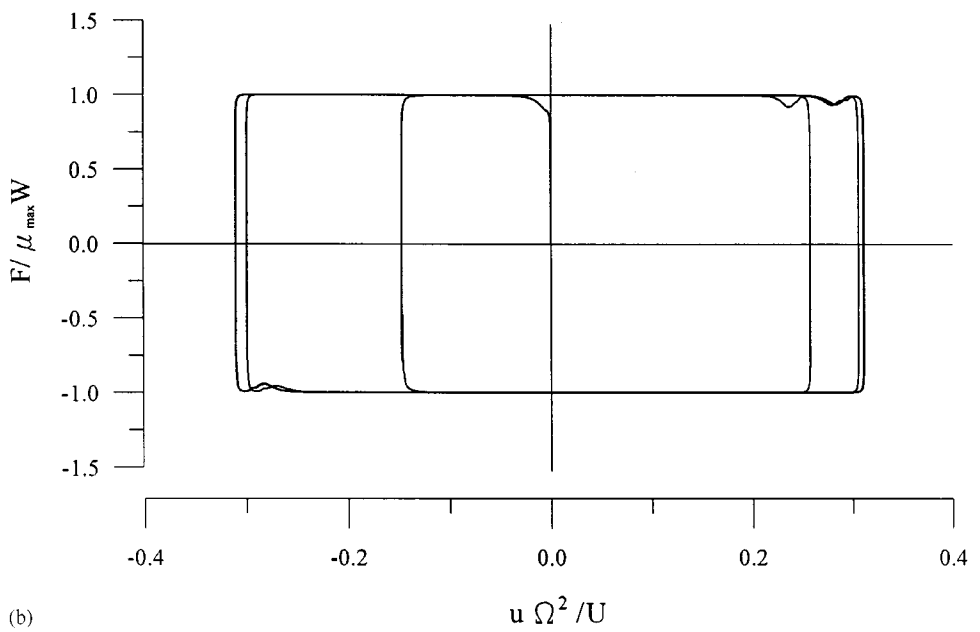

(b)

Figure 4. (a) Bearing displacement ($\Omega/\omega_1 = 0{\cdot}6$; $U/\mu g = 1$; Mokha's model); (b) Hysteresis of friction ($\Omega/\omega_1 = 0{\cdot}6$; $U/\mu g = 1$; Mokha's model)

When the bridge is excited under resonant condition ($\Omega/\omega_1 = 1$) with $U/\mu g = 1{\cdot}5$, for example, it is evident that the response tends to diverge with time. This result agrees with what has been indicated by Chopra[11] and Makris and Constantinou[12] that, the dynamic response for a Coulomb–friction–damped system diverges under resonant excitation if $U/\mu g > 4/\pi$. Moreover, sub-harmonic responses are observed from the normalized acceleration Fourier spectrum ($\ddot{u}/U$) of the bridge superstructure (Figure 5(b)). Interestingly, the peaks occur regularly at odd frequency ratios ($\omega/\Omega = 1, 3, 5, 7, \ldots$) as can be noticed. This familiar regularity

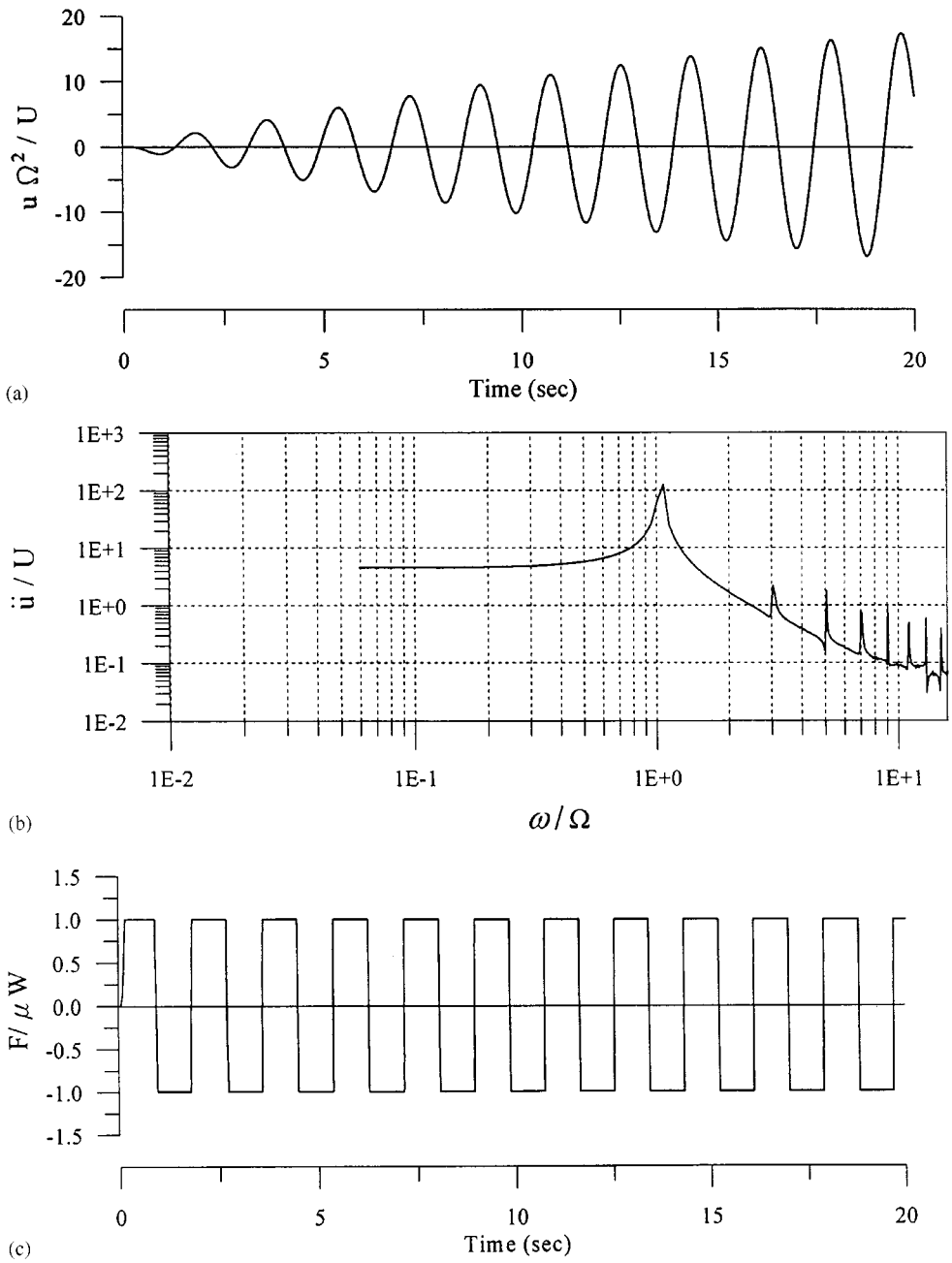

Figure 5. (a) Bearing displacement ($\Omega/\omega_1 = 1{\cdot}0$; $U/\mu g = 1{\cdot}5$); (b) Fourier spectrum of bridge acceleration ($\Omega/\omega_1 = 1{\cdot}0$; $U/\mu g = 1{\cdot}5$); (c) History of friction force ($\Omega/\omega_1 = 1.0$; $U/\mu g = 1{\cdot}5$)

is in fact consistent with the Fourier spectrum of a system subjected to periodic square waves. It is realized as soon as one investigates the time history of the normalized friction force ($F/\mu W$) in Figure 5(c) that, the forcing function appears to be nothing but a periodic square wave, except the transient portion before slippage initiates. This explains the sub-harmonic responses observed in sliding structures with Coulomb friction.

The integration time step Δt is crucial, in particular for non-linear dynamic analysis, to the convergence of numerical results. As a further step to investigate the effect of Δt value on the accuracy of the results, harmonic response analyses are carried out for various frequency ratios ($\Omega/\omega_1 = 1, 3, 5$) at different scale of time steps ($\Delta t = 0{\cdot}02, 0{\cdot}01, 0{\cdot}005, 0{\cdot}002$ sec). As the accuracy of the simulation results of sliding structures are

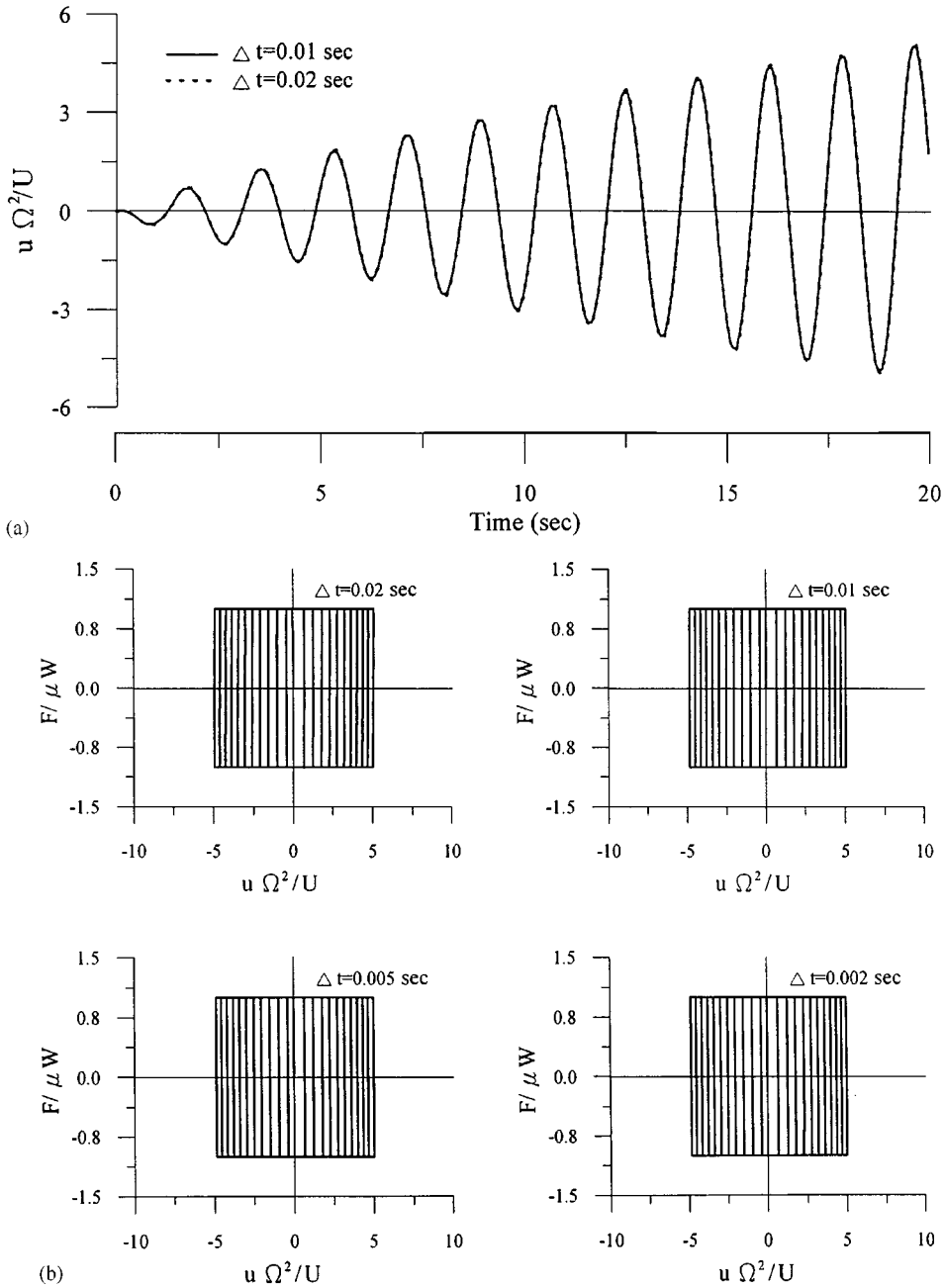

Figure 6. (a) Bearing displacement ($\Omega/\omega_1 = 1$; $U/\mu g = 1$; Coulomb's model); (b) Hysteresis of friction ($\Omega/\omega_1 = 1$; $U/\mu g = 1$; Coulomb's model)

most stringently revealed from the hysteresis of the friction force of a prescribed friction mechanism (e.g. Coulomb's model), these results are presented along with the sliding displacements of the isolation bearings. Figure 6(a) shows the bearing displacement under a resonant condition ($\Omega/\omega_1 = 1$) and Figure 6(b) shows the hysteresis of friction with respect to various Δt. The hysteresis shows the exact pattern of the Coulomb's

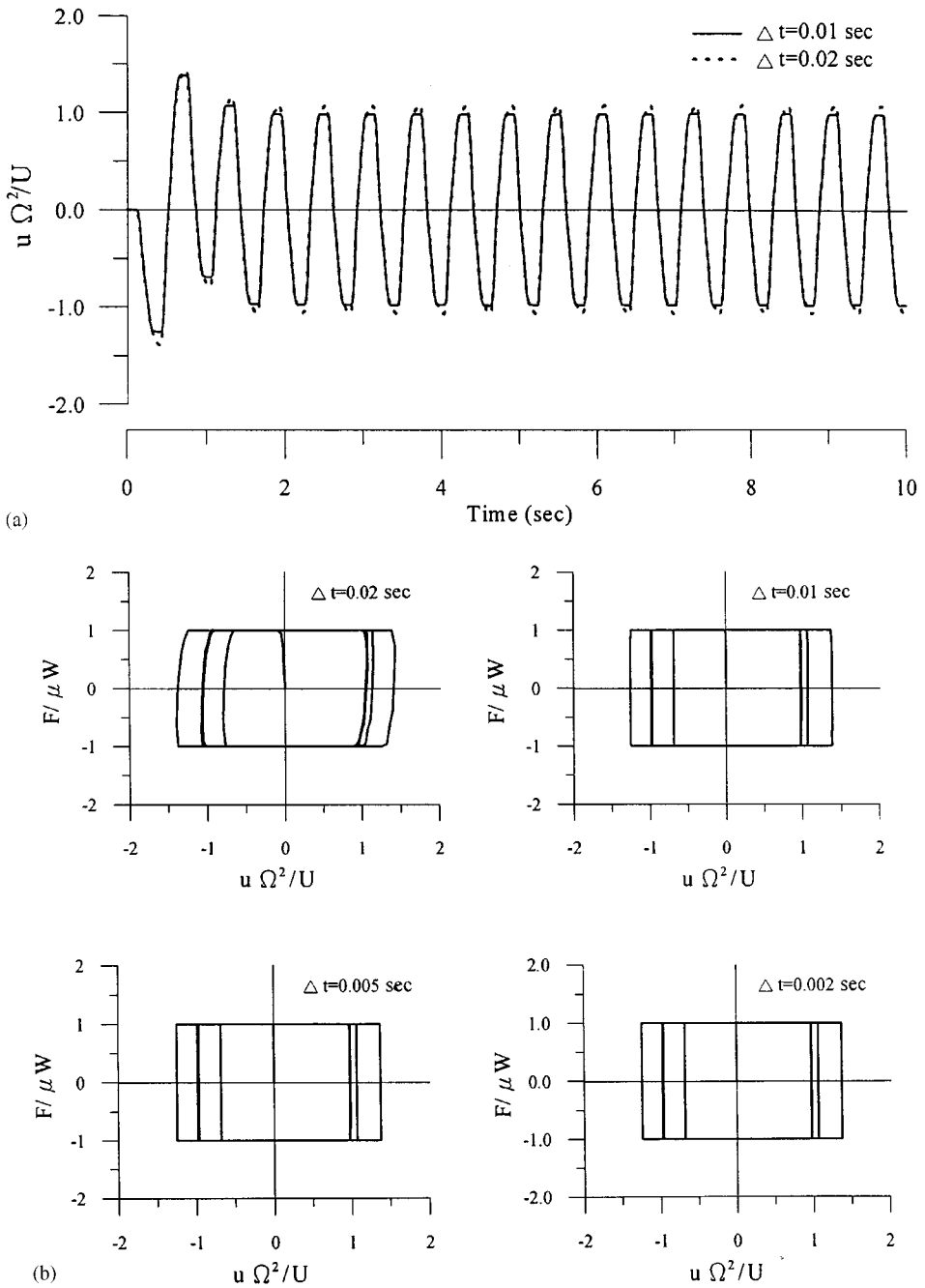

Figure 7. (a) Bearing displacement ($\Omega/\omega_1 = 3$; $U/\mu g = 1$; Coulomb's model); (b) Hysteresis of friction ($\Omega/\omega_1 = 3$; $U/\mu g = 1$; Coulomb's model)

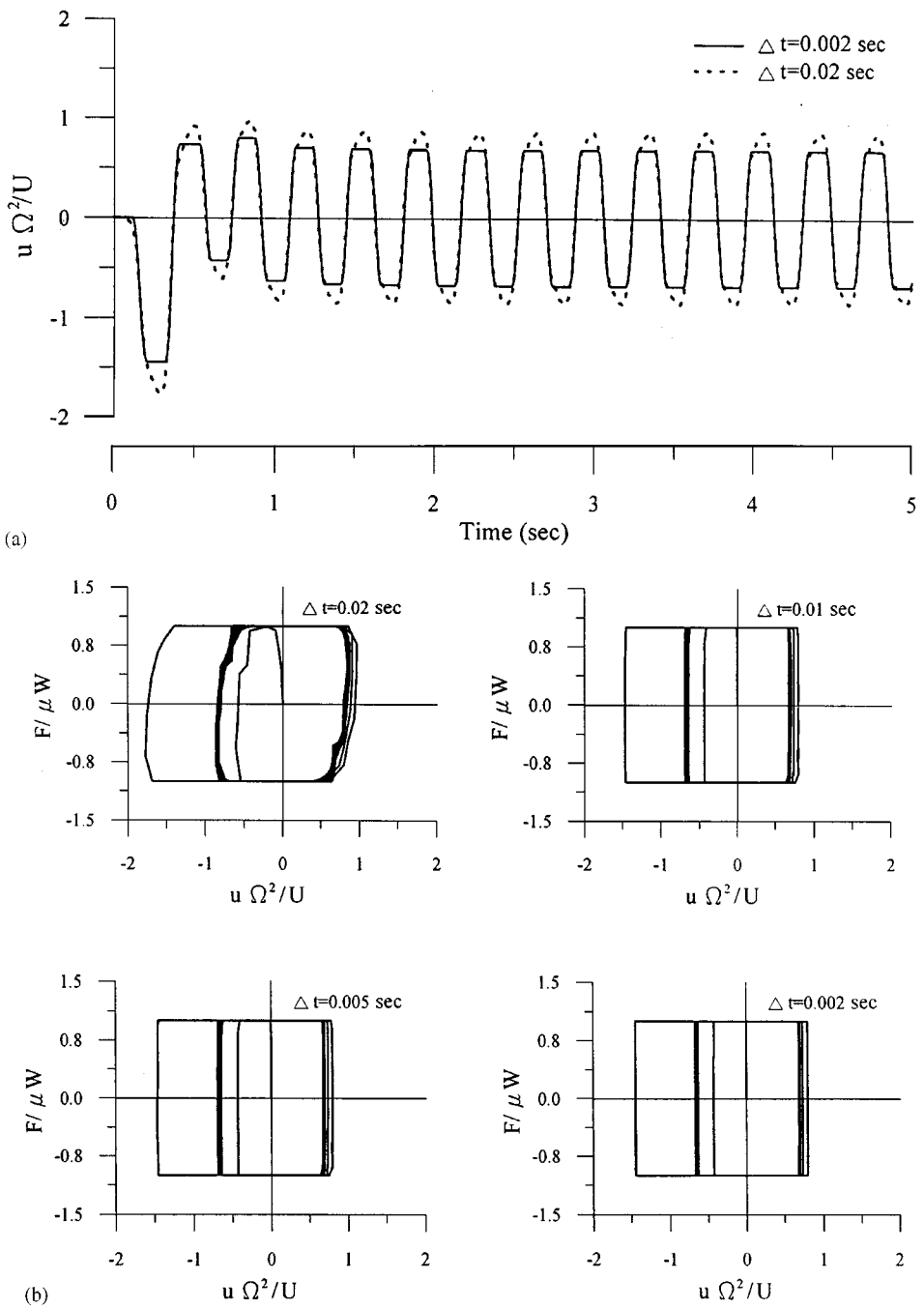

Figure 8. (a) Bearing displacement ($\Omega/\omega_1 = 5$; $U/\mu g = 1$; Coulomb's model); (b) Hysteresis of friction ($\Omega/\omega_1 = 5$; $U/\mu g = 1$; Coulomb's model)

friction at all the cases. When the exciting frequency is increased to $\Omega/\omega_1 = 3$, bending of the vertical lines of the hysteresis is visible in the case of $\Delta t = 0{\cdot}02$ sec as shown in Figure 7(b) which violates the prescribed friction model of Coulomb's, strictly speaking. This leads to the overshooting of the sliding displacement as indicated in Figure 7(a). However, the result converges at $\Delta t = 0{\cdot}01$ sec. When the exciting frequency

Table II. Effectiveness Assessment of Seismic Isolation

Max. Response Quantity*	Bridge Type		
	Conventional	Isolated w/o constraint	Isolated w/ constraint
(a) El Centro			
VP1(kN)	3461	274	176
VP2(kN)	3461	274	303
MP1(kN-m)	27486	2124	1270
MP2(kN-m)	27486	2124	2192
DP1(cm)	4·42	0·34	0·19
DP2(cm)	4·42	0·34	0·34
DB1(cm)	4·42	2·45	0·19
DB2(cm)	4·42	2·45	0·34
AR(kN)	0	0	4769
(b) Kobe			
VP1(kN)	17428	1933	211
VP2(kN)	17428	1933	318
MP1(kN-m)	138387	15573	1426
MP2(kN-m)	138387	15573	2268
DP1(cm)	22·24	2·52	0·21
DP2(cm)	22·24	2·52	0·34
DB1(cm)	22·24	40·70	0·21
DB2(cm)	22·24	40·70	0·34
AR(kN)	0	0	5131
(c) Mexico			
VP1(kN)	1321	2687	42
VP2(kN)	1321	2687	63
MP1(kN-m)	10480	21409	284
MP2(kN-m)	10480	21409	449
DP1(cm)	1·68	3·45	0·04
DP2(cm)	1·68	3·45	0·07
DB1(cm)	1·68	53·30	0·04
DB2(cm)	1·68	53·30	0·07
AR(kN)	0	0	1019

* VP1 = Shear of Pier 1, VP2 = Shear of Pier 2, MP1 = Moment of Pier1, MP2 = Moment of Pier 2, DP1 = Disp. of Pier 1, DP2 = Disp. of Pier 2, DB1 = Disp. of Bearing 1, DB2 = Disp. of Bearing 2, AR = Abutment Reaction

increased further to $\Omega/\omega_1 = 5$, the errors become more serious and the result converges when the integration time step is as small as $\Delta t = 0{\cdot}002$ sec, as observed from Figure 8(b). Distortion of the hysteresis is mainly due to the numerical errors introduced by the high-frequency modes of the structure of which the ratio $\Delta t/T_i > 0{\cdot}5$ for some i where T_i is the natural period of the ith mode.[13] Nevertheless, the value required for acceptable accuracy using the proposed algorithm is reasonable.

Response to earthquake excitations

The performances of FPB-isolated bridges under seismic loadings in the longitudinal direction are investigated. The objective of isolation of bridge structures is primarily to reduce the shear forces resisted by the piers that are most vulnerable during earthquakes. With the piers isolated from the bridge superstructure

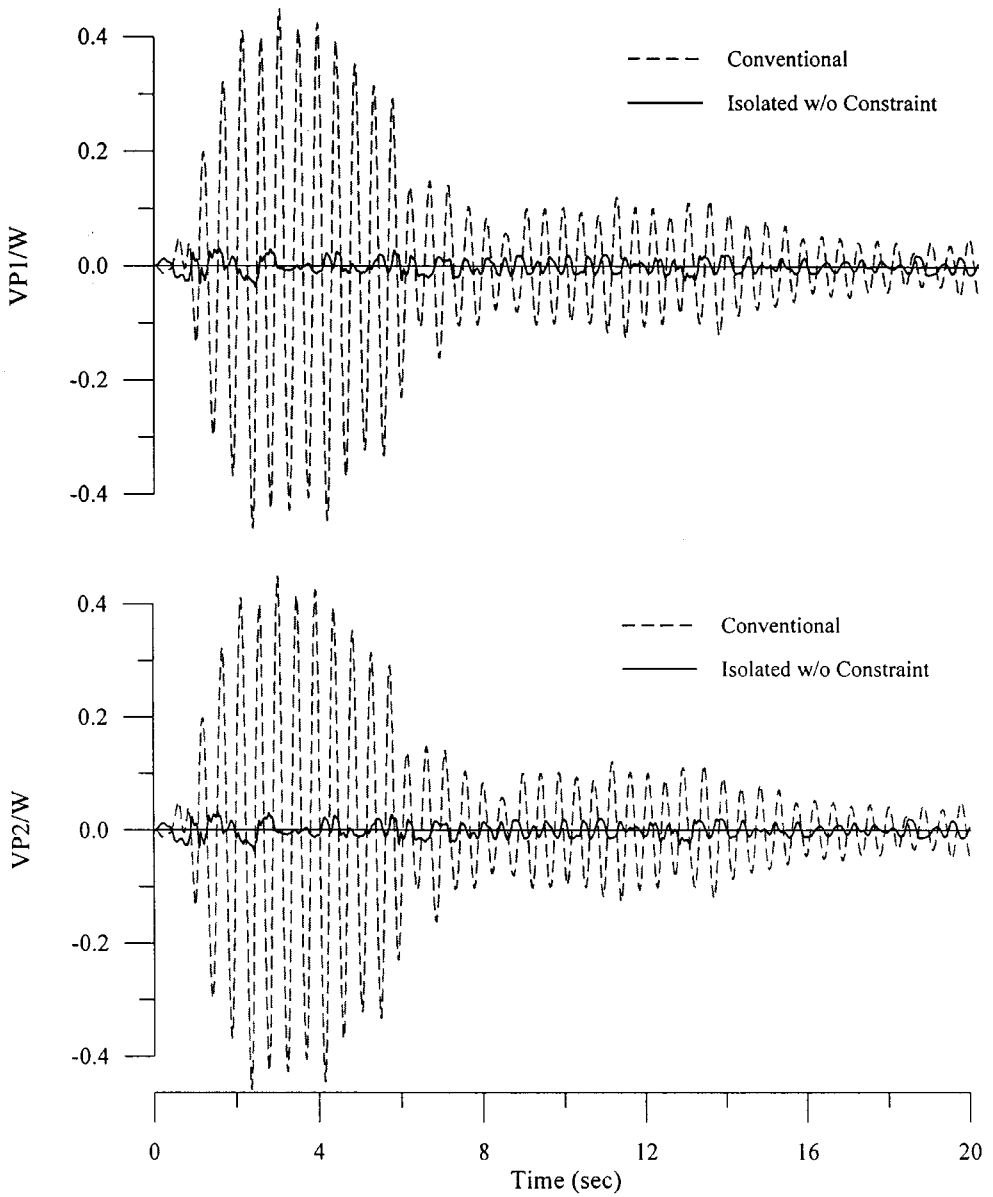

Figure 9. Shear force of the piers (El Centro)

using friction bearings, the bridge and the piers vibrate independently during the earthquake and thus interactions between them are minimized. However, due to a substantial discount of lateral stiffness after isolation, the superstructure is likely subjected to excessive slippage during the earthquake, as it is often encountered for building structures. This deficit is commonly improved by introducing additional damping or energy dissipation devices. Since bridges are structurally different from building systems, more alternatives are available other than appealing to energy dissipation. Actually, displacement constraint of the bridge superstructure can be provided by simply replacing one of the roller supports on the abutments with a hinge, as shown in Figure 2(c). With such a rearrangement on support conditions, however, the bridge is no longer

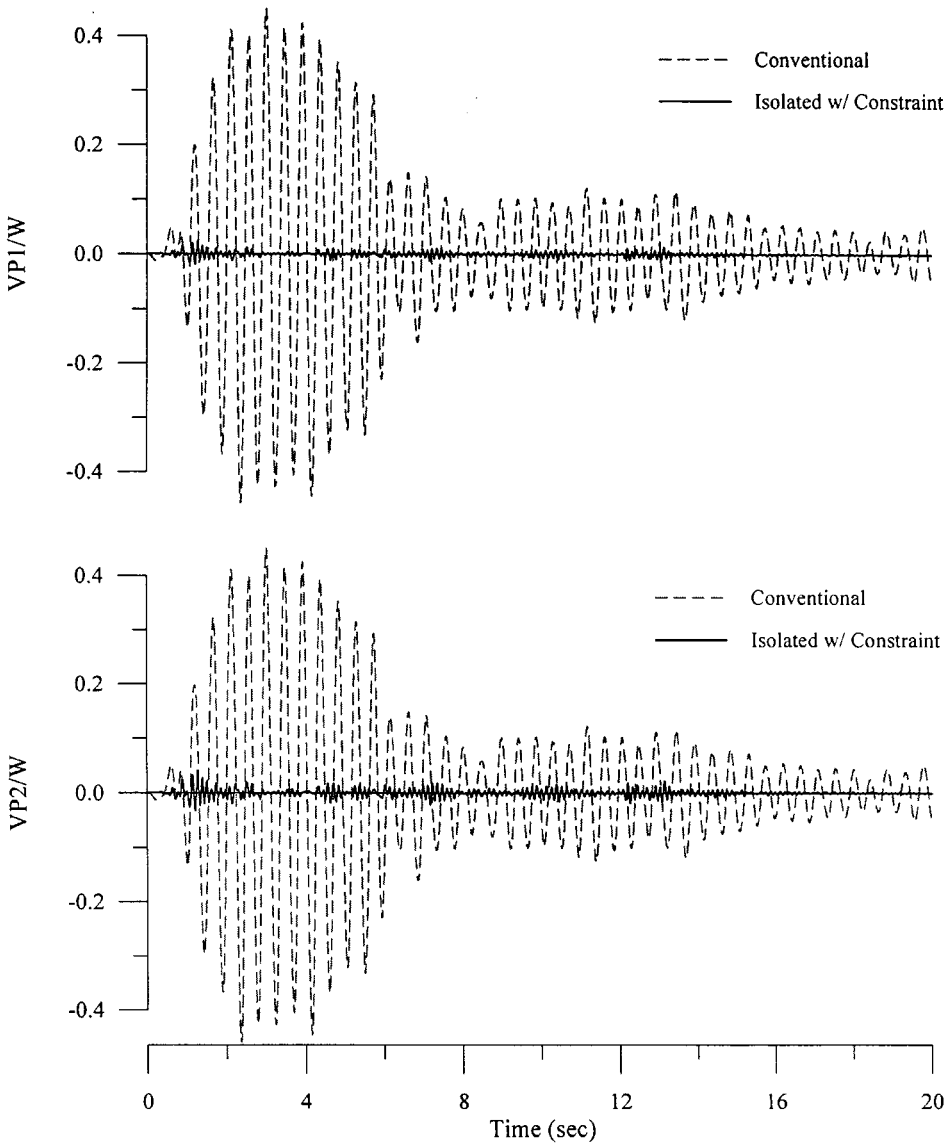

Figure 10. Effects of constraint on shear force of the piers (El Centro)

symmetric and the friction bearings behave independently along with the piers, as a consequence. This modification drastically changes the dynamic characteristic of the bridge system while increasing the complexity of the analysis task as a result. The proposed numerical scheme is adopted to deal with this situation.

Effectiveness assessment

To show the effectiveness of seismic isolation, structural responses of the isolated bridge to earthquakes, in particular, shear and moment at the pier foot along with bridge displacement at the bearing locations, are examined. In addition, reaction force at the abutment for the bridge in the revised configuration is also investigated. Simulations using the recorded earthquake ground motions of El Centro

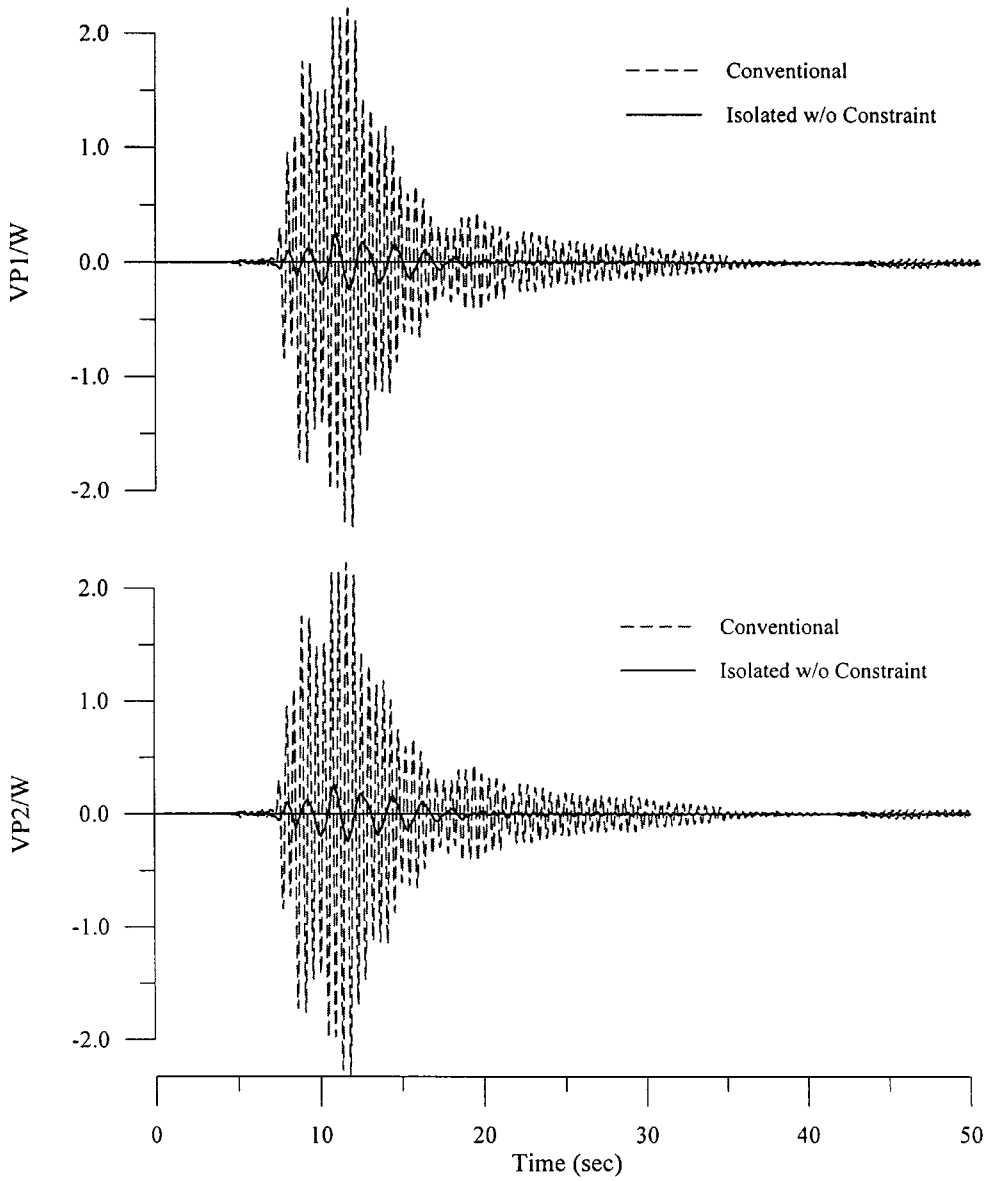

Figure 11. Shear force of the piers (Kobe)

(1940), Kobe (1995) and Mexico (1985) as inputs are presented in order to verify the adaptiveness of the isolated bridges under different geological conditions.

(a) *El Centro (PGA = 0·34g)*: The 1940 El Centro earthquake is typical for hard sites. Simulation results are summarized in Table II(a). Significant reductions for the piers' base shears of the isolated bridge without constraint are observed from the response time histories demonstrated in Figure 9, where the base shears are normalized with respect to the weight (W) of the bridge superstructure ($W = 7700$ kN). The maximum bearing displacement is 2·45 cm. When the bridge superstructure is constrained with a hinge support, the

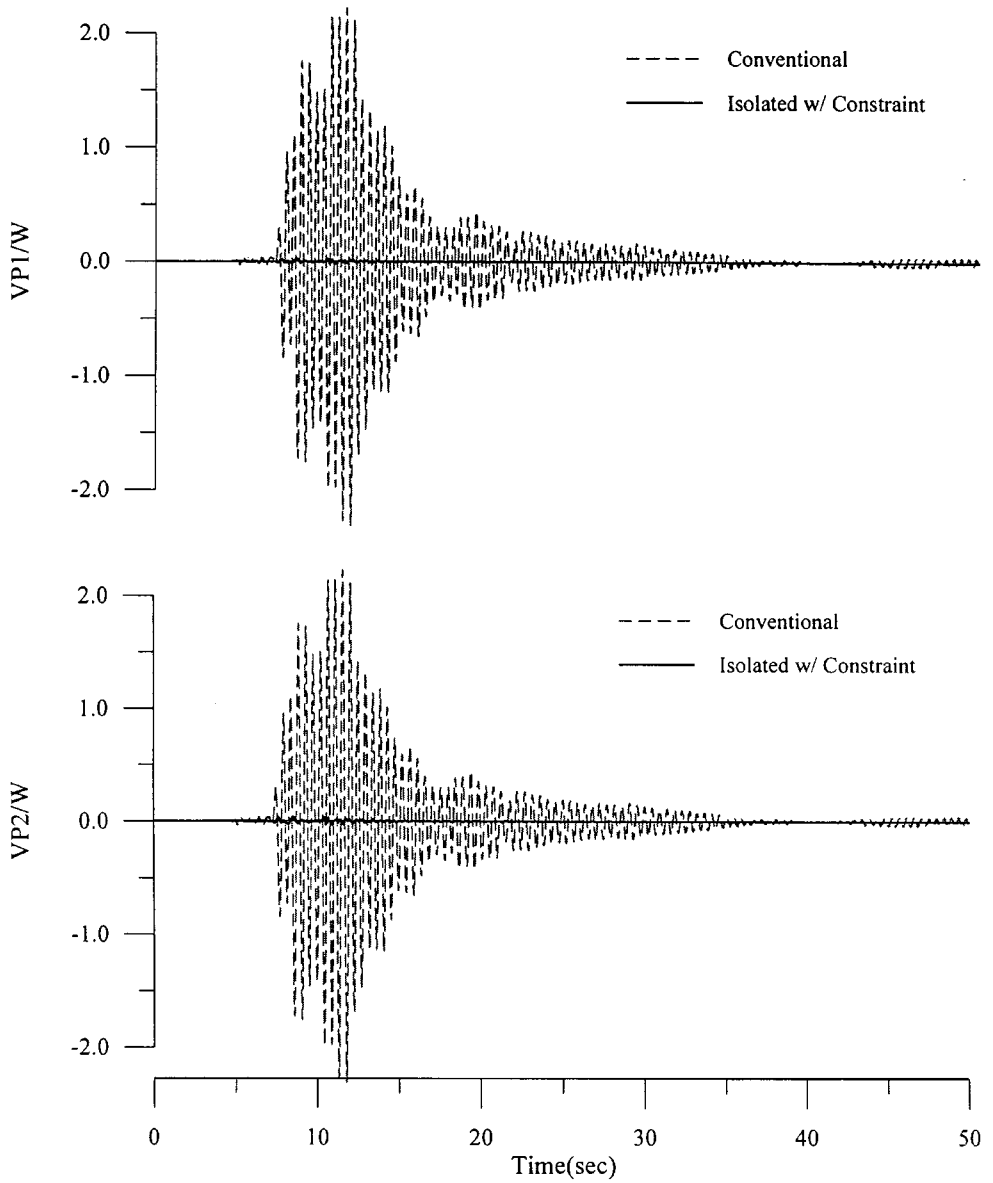

Figure 12. Effects of constraint on shear force of the piers (Kobe)

maximum bearing displacements are reduced, respectively, to 0·19 and 0·34 cm, and the pier's base shears are further reduced, as shown in Figure 10. Note that Pier1 takes notably less force than pier2 since its neighbouring abutment shares some loads. Peak reduction of shear force of 95 per cent is achieved for pier1 and 91 per cent for pier2. The piers' base moments are also significantly suppressed; their peaks are shown to be reduced by 94 per cent in average. These improvements in performance are, as a trade-off, associated with considerable reaction forces to the abutment on which the horizontal displacement constraint is provided. Normally, squat in shape and backed-up with land, the abutments are intrinsically much stiffer than piers; they can therefore accommodate comparatively more loads than piers. Special attention would then be paid

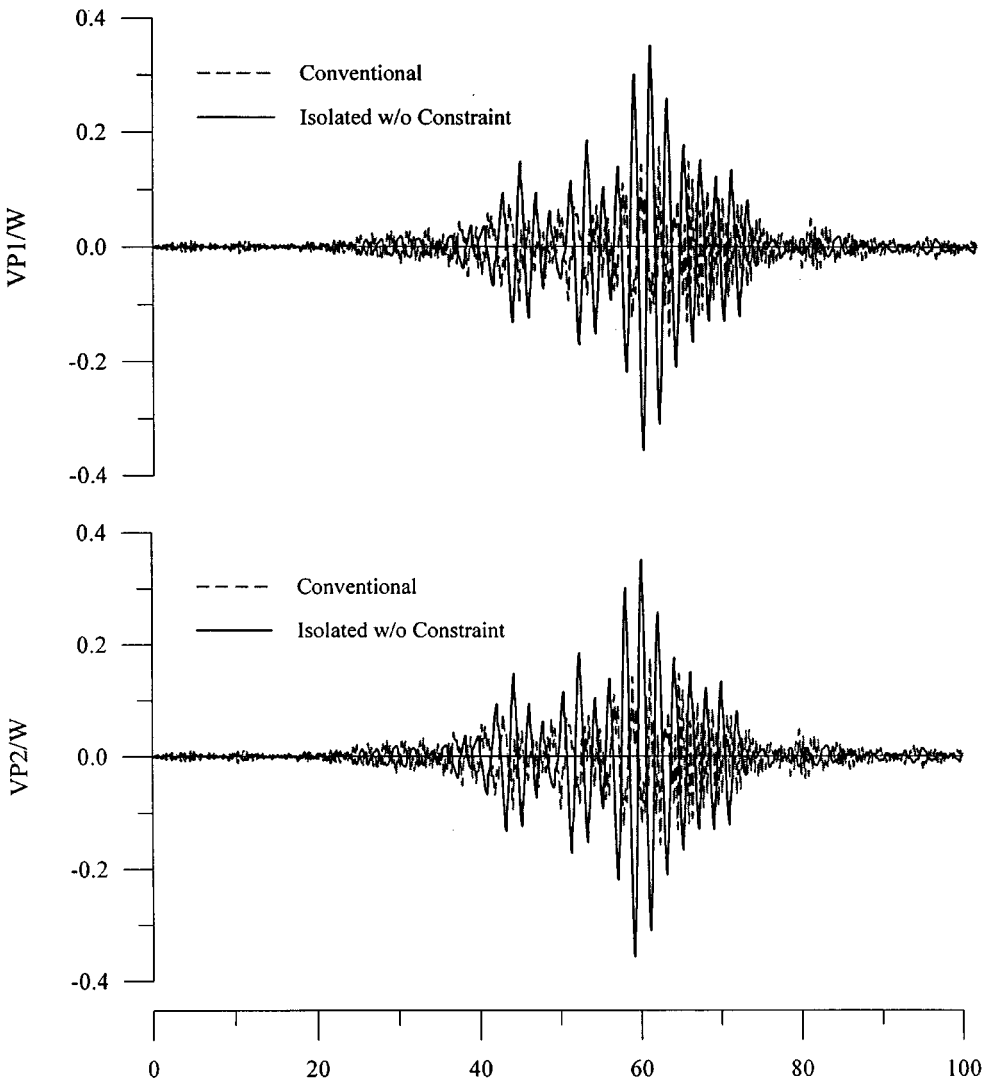

Figure 13. Shear force of the piers (Mexico)

to the lateral loading capacity of the hinge support as it would become critical in seismic isolation design.

(b) *Kobe earthquake (PGA = 0·83g)*: The 1995 Kobe earthquake is among the most destructive seismic events ever occurred worldwide. The scale of this earthquake is approximately five times of the 1940 El Centro earthquake in terms of the resulted peak structural responses of the conventional bridge, as revealed from Tables II(a) and II(b), assuming no damage in the structures. The isolated bridge without constraint again shows great performance in earthquake protection, as illustrated in Figure 11 for the piers' base shear. However, the maximum bearing displacement is over 40 cm in this case. When displacement constraint is considered, significant reduction of the normalized pier shears can be achieved, as illustrated in Figure 12. In fact, the peak reductions of all the structural responses indicated in Table II(b) are found to be approaching 99 per cent. Furthermore, the maximum bearing displacements are reduced from 40 to 0·21 and 0·34 cm, respectively for the two bearing at the expense of getting a maximum abutment reaction of 5131 kN. The advantage of applying displacement constraints for seismically isolated bridges is evident.

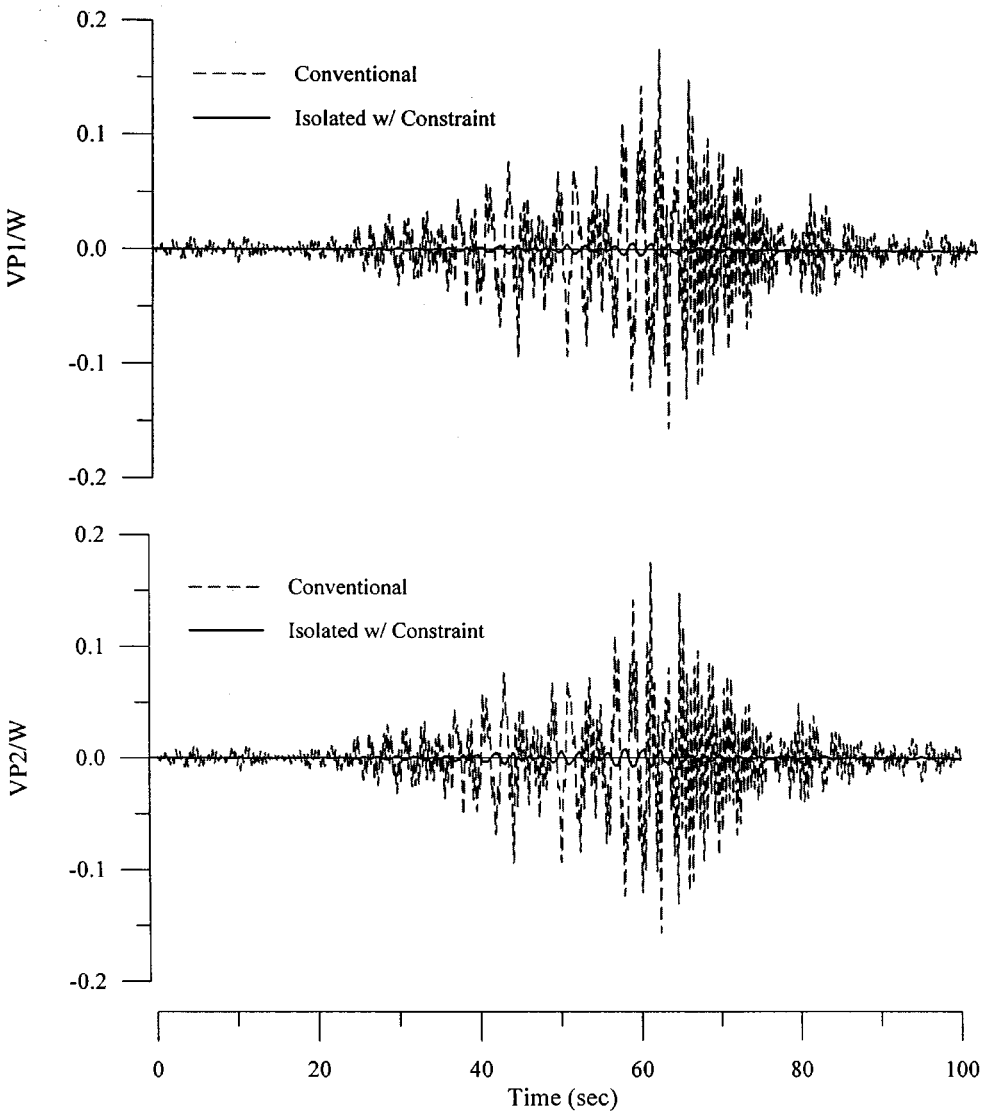

Figure 14. Effects of constraint on shear force of the piers (Mexico)

(c) *Mexico (PGA = 0·17g)*: The 1985 Mexico earthquake is a representative for soft sites. The frequency content of this earthquake is composed predominantly of a long vibrational period at 2 sec. Simulation results are summarized in Table II(c). When the bridge is isolated without constraint, the responses are twice as much amplified, as shown in the piers' base shear (Figure 13) due to resonance. Besides, the maximum bearing displacement is 53 cm which is practically unacceptable. However, if the displacement constraint is provided, performance of the isolated bridge is completely different. As demonstrated in Figure 14, the normalized pier shears of the isolated bridge with constraint are significantly reduced. The peaks of the pier shears and the pier base moments are drastically reduced by 96 per cent, as indicated in Table II(c). Furthermore, the bearing displacements are reduced from 53 cm to almost nothing. Normally, isolating structures in such areas would not be recommended since it could endanger the structures the other way around. This inference, however, does not apply to the isolated bridges with constraint as proposed.

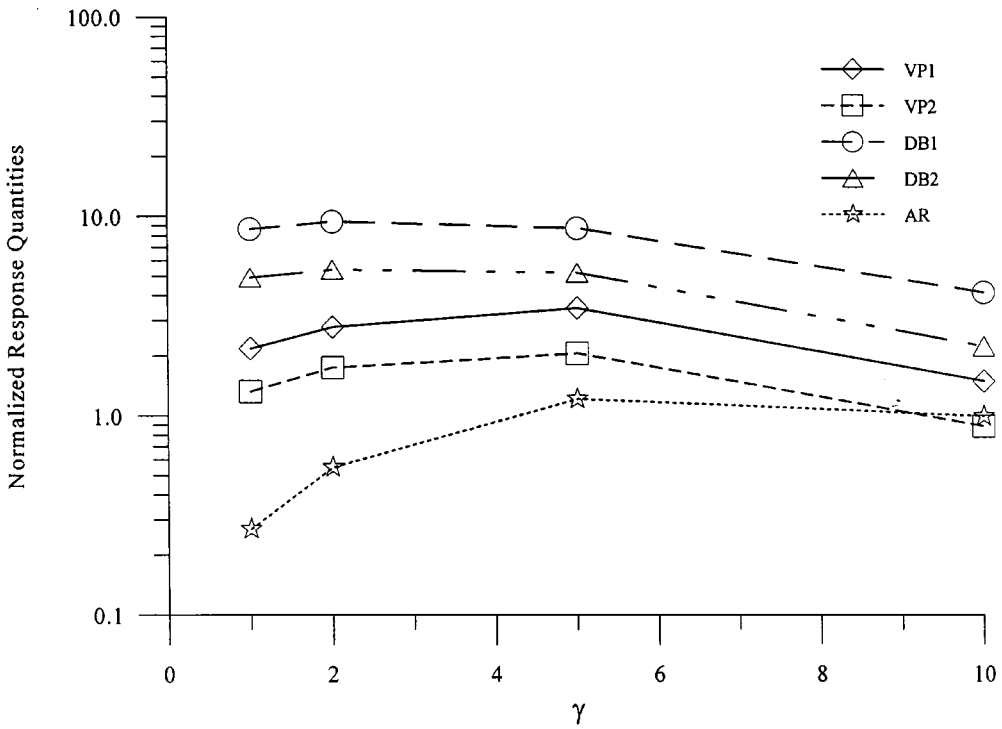

Figure 15. Effects of abutment flexibility (El Centro)

Emphasis should be placed on the substantial reduction in bearing's displacement, which can rarely be expected for an isolated structure. The hinge support contributes significantly in displacement control. The performance of such isolated bridges have been shown to be satisfactory.

Effects of Abutment's flexibility

In the previous analysis, the abutments are modelled to be infinitely stiff that no flexure is allowed to occur. The effect of abutment flexibility on the overall performance of the isolated bridge requires further investigation, even though the abutments are much more rigid than the piers in general. For elevated highway bridges, moreover, the hinge supports that provide displacement constraints of the isolated superstructure have to be implemented on the piers, inevitably.

Analyses are carried out for various abutment-to-pier stiffness ratios $\gamma = 1, 2, 5, 10, \infty$. The response quantities normalized with respect to those of the idealized case ($\gamma = \infty$) are presented, respectively, in Figures 15–17 for El Centro, Mexico and Kobe earthquakes. The maximum bridge displacements at the bearing locations (DB1,DB2) are increased almost monotonously as the abutment's stiffness decreased. Amplification of bridge displacement are evident for low stiffness ratios. However, the actual maximum displacement in the extreme case ($\gamma = 1$, Kobe earthquake) is below 12 cm, which practically can be accommodated by the expansion joint. Variation of the pier's shear forces (VP1, VP2) follows a similar pattern, except in El Centro earthquake where no specific trend is observed. Deviations of the shear forces from the idealized one in all three cases are considerably less though, compared with the bridge displacements. The abutment reaction (AR), in general, tends to be decreased as the stiffness decreased while the structure undergoing larger deformation as a trade-off, except in Kobe earthquake. Nevertheless, deviations of the abutment reaction from the idealized one are the least in comparison with the other response quantities.

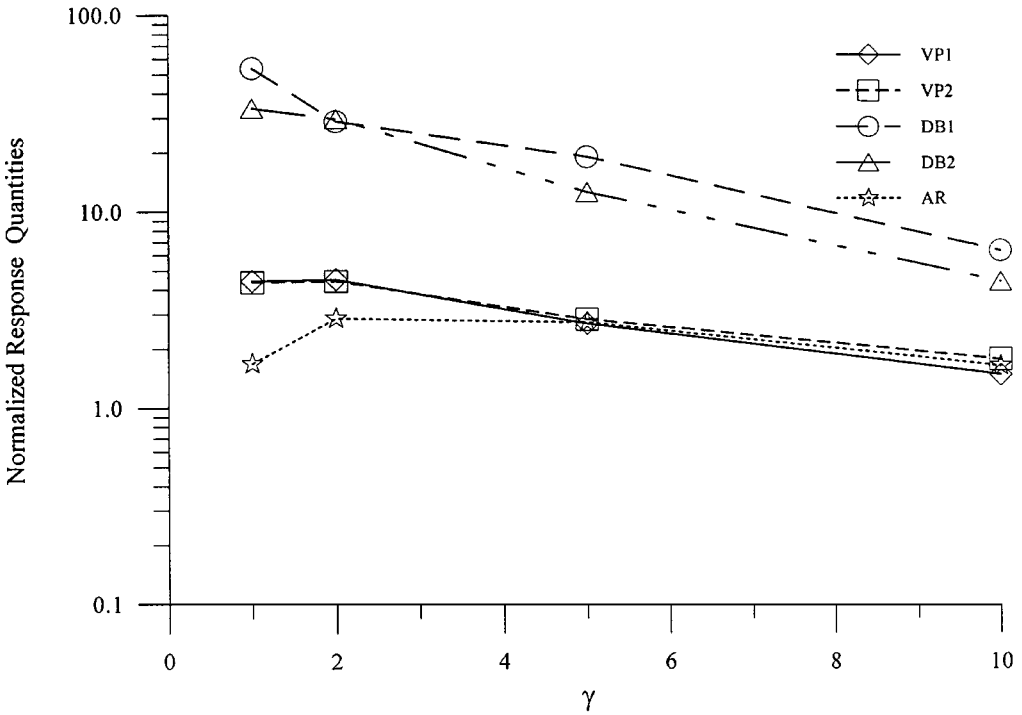

Figure 16. Effects of abutment flexibility (Kobe)

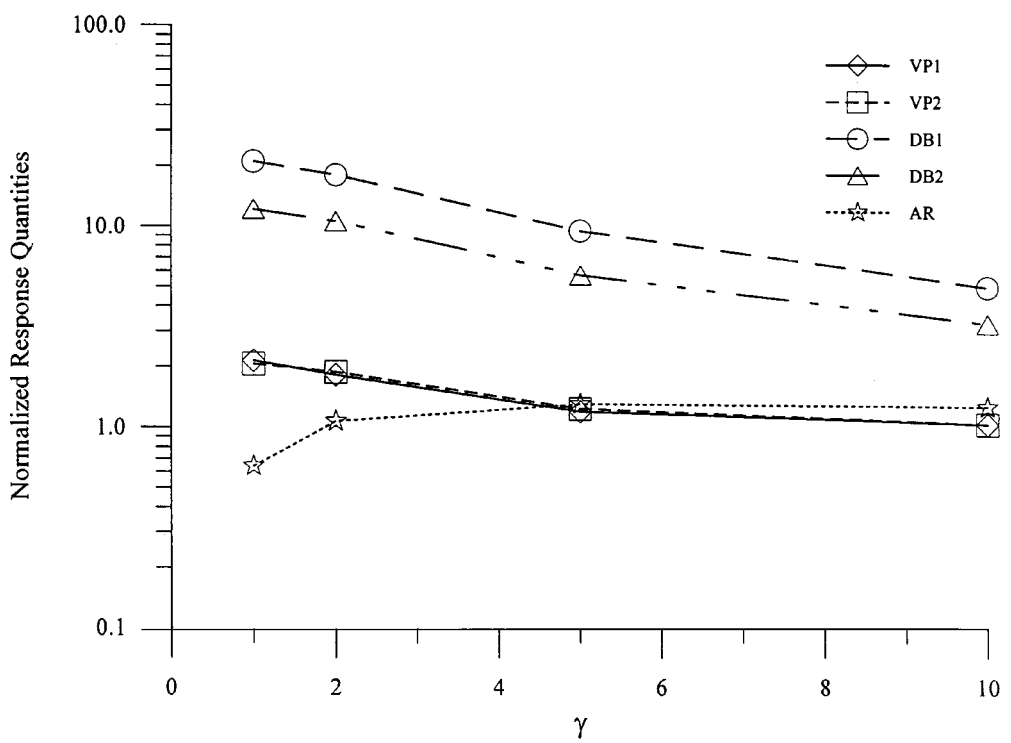

Figure 17. Effects of abutment flexibility (Mexico)

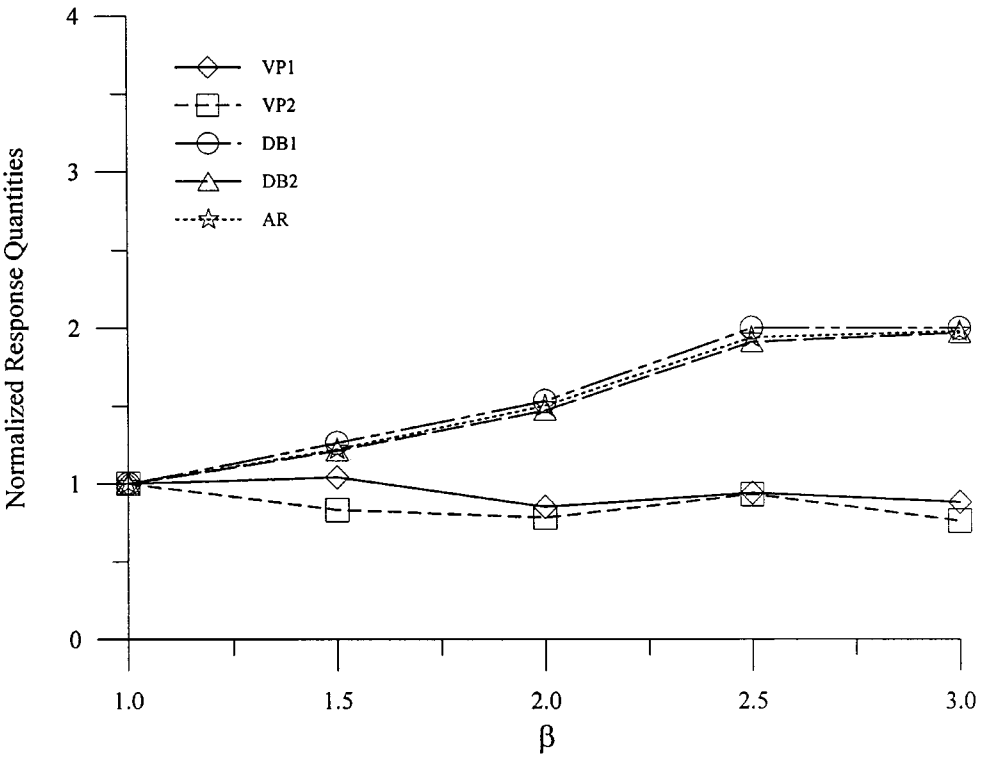

Figure 18. Effects of bridge weight (El Centro)

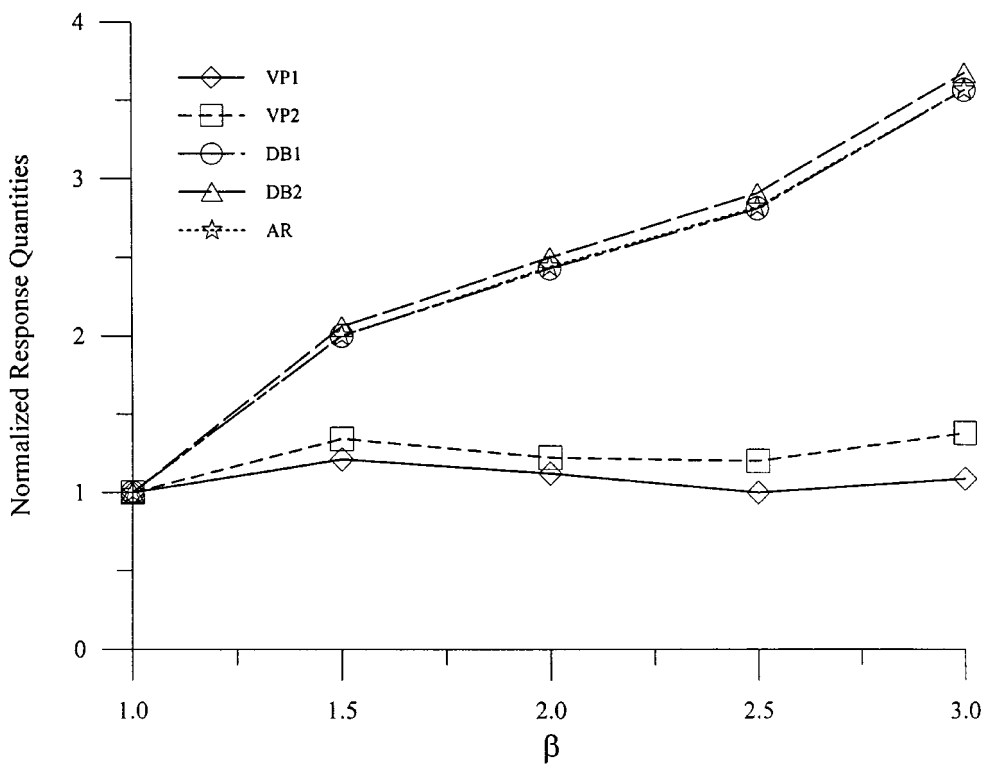

Figure 19. Effects of bridge weight (Kobe)

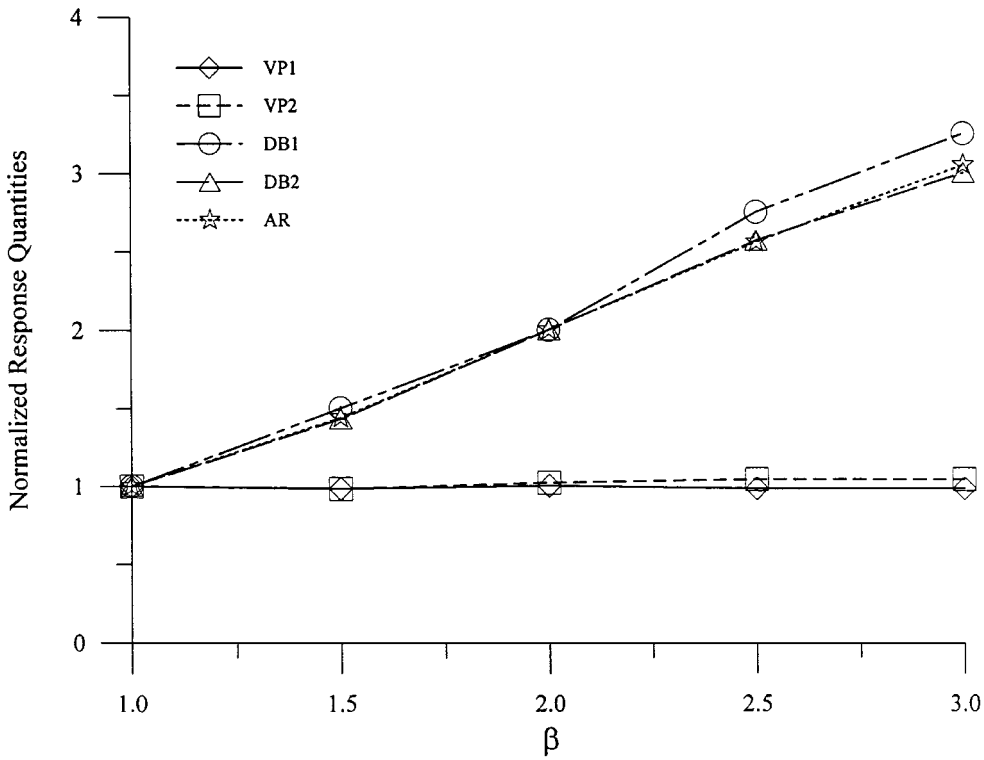

Figure 20. Effects of bridge weight (Mexico)

Effect of bridge's weight

The unit weight of the bridge superstructure considered in the analytical model is originally 8·6 t/m, which corresponds to light-weight bridges practically. The effect of bridge's weight on the overall performance of the isolated bridges therefore requires further investigations.

Simulations are carried out for bridges from light-weight to heavy-weight with weight ratios (β) from 1 to 3. The response quantities normalized with respect to those of the light-weight case ($\beta = 1$) are presented, respectively, in Figures 18–20 for El Centro, Mexico and Kobe earthquakes. The maximum bridge displacements at the bearing locations (DB1,DB2) and the abutment reaction forces (AR) increase with the bridge's weight, while the pier's shears (VP1, VP2) remain nearly unity with only slight variations in all the cases consistently. The inertia forces of the bridge superstructure induced during the earthquakes are almost fully transferred to the abutment regardless of bridge's weight. The insensitivity of the pier's responses to bridge's weight is due to the load-filtering capability of the non-linear friction mechanism provided by the isolation bearings through the threshold of the maximum friction force.

CONCLUSIONS

A simple as yet efficient solution algorithm for non-linear dynamic analysis of sliding structures has been proposed, based on the concept of shear balance at the sliding interfaces following a prescribed friction mechanism. The integration time step keeps constant without being chopped into infinitesimal pieces even during the transitions between sliding and non-sliding modes of the system. Adequacy of the proposed numerical procedure has been verified through harmonic responses of an isolated bridge under Coulomb's

friction model as well as Mokha's. Feasibility of using friction pendulum bearings for seismic isolation of bridges has been investigated under real earthquakes. Simulation results indicate that, at hard-soil sites, responses of the isolated bridges without constraint can be drastically reduced with acceptable bearing displacements. While at soft-soil sites, responses of the isolated bridge can be amplified and the bearings displace excessively, if the bridge superstructure stays entirely unconstrained. It is suggested in this study to resolve the dilemma by replacing one of the roller supports on the abutments with a hinge to provide displacement constraints, at the expense of increasing abutment's loading as a trade-off. Under the revised configuration, the isolated bridge performs consistently well during various earthquakes, regardless of the site conditions. The usefulness of seismic isolation of bridges is confirmed.

ACKNOWLEDGEMENT

This research is sponsored by the National Science Council of the Republic of China under Grant no. NSC 84-2221-E-009-008.

REFERENCES

1. I. G. Buckle and R. L. Mayes, 'Seismic isolation history: application and performance — a world review', *Earthquake Spectra* **6,** 161–201 (1990).
2. V. Zayas, S. S. Low and S. A. Main, 'The FPS earthquake resisting system, experimental report', *report no. UCB'EERC-87/01*, Earthquake Engineering Research Center, University of California, Berkeley, CA., June 1987.
3. S. Kawamura, K. Kitazawa, M. Hisano and I. Nagashima, 'Study of a sliding—type base isolation system – system composition and element properties', *Proc. 9th WCEE*, Tokyo-Kyoto, Vol. **V**, 1988, pp. 735–740.
4. M. C. Constantinou, P. Tsopelas, Y.-S. Kim and S. Okamoto, 'NCEER-Taisei corporation research program on sliding seismic isolation systems for bridges: experimental and analytical study of a friction pendulum system (FPS)', *Technical Report NCEER-93-0020*, NCEER, SUNY/Buffalo, 1993.
5. B. Westermo and F. Udwadia, 'Periodic response of a sliding oscillator system to harmonic excitation', *Earthquake Engrg. Struct. Dyn.* **11,** 135–146 (1983).
6. N. Mostaghel, M. Hejazi and J. Tanbakuchi, 'Response of sliding structures to harmonic support motion', *Earthquake Engrg. Struct. Dyn.* **11,** 355–366 (1983).
7. N. Mostaghel and J. Tanbakuchi, 'Response of sliding structures to earthquake support motion', *Earthquake Engrg. Struct. Dyn.* **11,** 729–748 (1983).
8. Y. B. Yang, T. Y. Lee and I. C. Tsai, 'Response of multi-degree-of-freedom structure with sliding supports', *Earthquake Engrg. Struct. Dyn.* **19,** 739–752 (1990).
9. A. S. Mokha, Constantinou, M. C. and A. M. Reinhorn, 'Teflon bearing in base isolation. I: testing', *J. Struct. Engrg.* ASCE **116,** 438–454 (1990).
10. A. S. Mokha, M. C. Constantinou and A. M. Reinhorn, 'Teflon bearing in base isolation. I: testing', *J. Struct. Engrg.* ASCE **116,** 438–454 (1990).
11. A. K. Chopra, '*Dynamics of Structures — Theory and Applications to Earthquake Engineering*', Prentice-Hall, Englewood Cliffs, NJ, (1995).
12. N. Makris and M. C. Constantinou, 'Analysis of motion resisted by friction. I: constant Coulomb and linear/Coulomb friction', *Mech. Struct. Mach.* **19,** 477–500 (1991).
13. Chung, L. L., Wang, Y. P. and Yang, C. S. 'Stability and accuracy of numerical analysis for structural dynamics', *Engrg Struct.*, submitted.

